ASME Journal of Turbomachinery
Online journal at:
https://asmedigitalcollection.asme.org/turbomachinery

The Effects of Channel Supplies on Overall Film-Cooling Effectiveness

Emma M. Veley[1]
Department of Mechanical Engineering,
Pennsylvania State University,
State College, PA 16801
e-mails: emv53@psu.edu;
emma.veley@gwu.edu

Karen A. Thole
Department of Mechanical Engineering,
Pennsylvania State University,
State College, PA 16801
e-mail: kthole@psu.edu

David G. Bogard
Department of Mechanical Engineering,
University of Texas at Austin,
Austin, TX 78712
e-mail: dbogard@mail.utexas.edu

Cooling components in the hot section of a gas turbine are essential to component durability. Common methods of cooling include rib turbulators in internal passages and film cooling on external surfaces. The holes that produce the film cooling are fed from the internal channels often containing ribs. Consequently, there is an interdependence of internal heat transfer and external film cooling. The purpose of this study was to obtain a better understanding of the interaction of ribs and film cooling. To quantify the cooling performance, the surface temperatures were measured, from which overall effectiveness was calculated. For the experiments, additively manufactured test coupons were made of Inconel 718 to match engine Biot numbers. These test coupons had internal feed channels with and without ribs and had both cylindrical holes and meter-diffuser-shaped holes with 15 deg lateral expansion angles and a 1 deg forward expansion angle. A single rectangular channel was one type of feed channel. The other type of feed channel was individual circular channels, with each circular channel supplying an individual film-cooling hole. The experimental results showed that the circular individual channels have 80% higher baseline overall effectiveness than the single rectangular channels without any film cooling. Ribbed turbulators without film cooling also increased the overall effectiveness by 21% for single rectangular channels and by 29% for the circular individual channels compared to the respective non-ribbed channels. While the film cooling increased the overall effectiveness of all geometries, the single rectangular channels had increased overall effectiveness levels by up to twice that of the no film-cooling case. On average, the single rectangular channels had an 80% improvement from film cooling, whereas the individual channel feeds, on average, had only a 50% improvement, given their high baseline effectiveness levels. [DOI: 10.1115/1.4063927]

Keyword: heat transfer and film cooling

1 Introduction

To attain high thermal efficiency, the modern gas turbine engine operates with turbine inlet temperatures that exceed the softening temperature of the hot-section hardware. Consequently, the hot-section hardware must be convectively cooled. For the blades and vanes of the turbine, cooling air passes through internal channels and then through film-cooling holes on the surface that provide convective cooling through the hole as well as a relatively cool film along the airfoil.

The internal supply channels for the film-cooling holes have been shown to affect the coolant flow field through the holes, which subsequently affects the overall cooling effectiveness of the film [1–4]. These effects can be even more dramatic when considering a micro-channel supply to the film-cooling holes. Micro-channels, also known as double-wall cooling, are highly effective in cooling blade surfaces and expand the opportunities to use a range of channel geometries and internal cooling features. Ribs are often incorporated into these internal channels to increase internal convection [2,5,6].

This study seeks to determine how both the internal channel shape and ribs affect overall film-cooling performance. To determine the effect, both experiments and computational simulations were conducted, where two types of cooling holes, a cylindrical hole and a meter-diffuser-shaped hole, were fed by four different types of co-flow feed channels. Two of the four feed channels were a single rectangular channel, one of the two without ribs and one of the two with ribs. The other two of the four types of feed channels were circular channels that each fed a single cooling hole, with one channel type having ribs and the other channel type not having ribs. From these assorted geometries, the overall effectiveness and the numerical simulation results were used to determine the impact of the supply channel geometry on the cooling performance.

2 Literature Review

The supply channel for a film-cooling hole has been identified in former research as a critical component of determining film-cooling performance [1,2]. Previous studies have assessed the flow field of

[1]Corresponding author.

Manuscript received October 16, 2023; final manuscript received October 23, 2023; published online November 16, 2023. Assoc. Editor: Jerzy T. Sawicki.

the cooling jet and cooling performance resulting from the differences in supply from the type of fed, specifically quiescent plenum or cross-flow-fed holes [2,3], from the internal supply flow direction relative to the mainstream [3,4,7–10], from different internal velocities [3,11], and even from the effect of ribs [2,5,6,12]. Variations in the supply affect the flow structure at the inlet of the cooling hole, which consequently affects the cooling jet and cooling performance [1,3,4,13,14]. However, most prior studies have exclusively used a single rectangular supply channel [1–9,11–16].

Ribs, which are a common internal heat transfer augmentation feature, have been well researched as a stand-alone feature [17–19] and researched in conjunction with film-cooling holes [20,21]. Cooling schemes that incorporate both ribs and cooling holes have fundamentally different performances than using each feature individually.

Most studies that have examined both ribs and film cooling can be placed in one of two categories: internal effects or external effects. For internal effects, studies have reported on the effects in the supply channel from coolant being removed through the film-cooling holes but do not report the film-cooling effectiveness [22–25]. For external effects, the studies focus on the effects of ribs on the external coolant jet as quantified by adiabatic or overall effectiveness [12,20,21,26–29]. Some of the external effects studies also assess the internal flow structure to determine the effects on the external cooling performance [12,21].

By examining a wide range of rib configurations with cross-flow-fed film-cooling holes, Sakai and Takahashi [21] determined that having ribs oriented to guide the flow toward the cooling hole axis improved the adiabatic film-cooling effectiveness, especially at low blowing ratios. Conversely, ribs that guided the flow counter to the cooling hole flow direction caused the adiabatic effectiveness to be lower than if the holes were fed from a channel with no ribs [21]. These rib orientation results were corroborated in a later experimental study by Klavetter et al. [27]. Similarly, Agata et al. [26] performed a detached eddy simulation for both rib orientations to find that the ribs that guided the flow counter to the cooling hole flow (backward) resulted in a swirling flow at the hole entrance that was maintained through the cooling hole. The resulting coolant jet had asymmetric flow structures that caused uneven cooling on the surface. The rib that guided the flow in the mainstream direction also caused a swirling flow through the cooling hole, but the swirling was weaker than it was in the backward rib, producing a coolant jet that was not significantly skewed [26].

Krille et al. [30] created several additively manufactured (AM) channels with ribs. The resulting surface topology of the channels and ribs was dependent on the build orientation. Consequently, the authors could analyze channels with varying stochastic surface roughness and varying artificial roughness from the ribs. The local Nusselt number results showed that the rib density impacted the heat transfer performance more than variations in surface roughness [30].

Additive manufacturing provides a relatively quick method for prototyping and testing cooling designs. There have been several studies that have used AM to create and test film-cooling holes at engine-relevant scales [8,15,31–33]. Additively manufactured cooling holes have notable roughness within the hole, which decreases the film-cooling effectiveness compared to a smooth hole created through electrical discharge machining (EDM) [15] but increases the in-hole convection compared to smooth holes [15]. The benefit from the speed and the cost of AM is valuable when investigating unique designs, such as hole geometries designed through optimization processes. This benefit from AM has been taken advantage of in several studies [8,32,33], one of which was a study that examined the effect of coolant feed direction in additively manufactured coupons [8]. In an early study in terms of using AM for manufacturing film-cooling holes, Stimpson et al. [8] found that when the flow is supplied in the counter-flow direction, the film-cooling performance is degraded compared to when fed by co-flow for the relatively smooth holes ($R_a/D_h \leq 0.1$). For relatively rough holes ($R_a/D_h > 0.1$), the mixing induced by the roughness was found to decrease the impact of the feed direction's overall effectiveness [8].

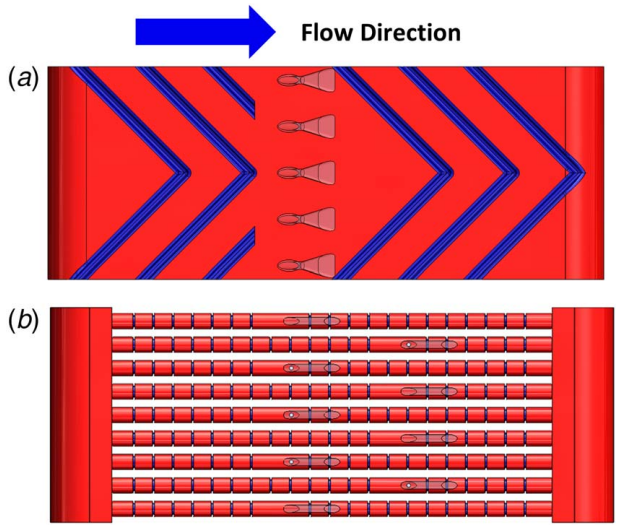

Fig. 1 Top views of the coolant gas path for (*a*) the single channel with Λ-Ribs and 15-15-1 holes and for (*b*) the individual channels with ribs and cylindrical holes

The study reported in this paper uses two hole shapes—the classic cylindrical hole and an "optimized" 15-15-1 [34] hole—to explore the cooling performance effects of supply channel shape and of ribs on the cooling performance. Specifically, two types of supply channel shapes will be discussed: a single rectangular channel and circular individual channels. Both channel types had cases that included and did not include ribs. Overall, effectiveness experiments were conducted using additively manufactured coupons with engine-scaled holes. Numerical conjugate heat transfer simulations were also conducted to better understand the internal flow physics.

3 Description of Geometries

For this study, test coupons were designed and additively manufactured at a scale relevant to aircraft hot-section hardware. A total of 12 test coupons were created with the goal of examining the interdependence of internal channel shape, ribs, and film-cooling hole shape on the overall cooling effectiveness.

Each test coupon had one of two feed channel shapes, as seen in Figs. 1(*a*) and 1(*b*): a single rectangular feed channel, which will be known as a single channel, feeds all the holes; individual circular feed channels, which will be known as individual channels,

Table 1 Geometric parameters of the feed channels

Parameter	Single	Individual
Channel shape	Rectangular	Circular
Channels	1	9
D_h (mm)	4.61	1.52
W/H	8.1	1
S/D_h	–	1.5
H/D	3.4	2
Ribs	45 deg Λ-ribs	90 deg ribs
Rib cross section	Filleted square	Square
e/H	0.25	0.125
P/e	10	10
R/e	0.5	–
X/D rib before hole	−11.0	−11.7
X/D rib after hole	14.5	−3.7

Table 2 Geometric parameters of the cooling holes

Hole shapes	D (mm)	P/D in row	P/D between rows	2nd row X/D	X/D 1st row inlet	t/P	L/D	L_m/D	β_{lat}	β_{fwd}
Cylindrical	0.762	6	3	15	−7.2	0.167	6	6	–	–
15-15-1	0.762	6	3	15	−7.4	0.505	6	2.5	15 deg	1 deg

separately feed each individual film-cooling hole. Table 1 enumerates the geometric parameters of the feed channels and ribs in both types of channels. The external film-cooled wall thickness (t_{wall} = 2.3 mm) was maintained for each internal channel design. The rectangular cross section of the single channel had a channel height (H) of 3.4 cooling hole metering diameters (D), which resulted in an aspect ratio (W/H) of 8.1. The nine circular individual channel supplies had diameters twice that of the cooling holes ($2D$). The individual channels were spaced three metering diameters ($3D$) apart.

Half of the six-single channel coupons had 45 deg Λ-shaped ribs. Figure 1 shows examples of two designs, one of which is the single channel with ribs. The 45 deg Λ-shaped ribs were placed on the top wall (film-cooled wall) of the internal channel. The Λ-shaped ribs were selected and designed with fillets to increase the printability on the downskin side of the channel. The radii of the fillets on the Λ-shaped ribs were selected based on work done by Rallabandi et al. [35].

Half of the six individual channel coupons had ribs. The ribs had square cross sections and wrapped around the entire circumference of the channel, as shown in Fig. 1(*b*). The rib design has been previously studied at a larger scale in rib roughened tubes [36], which was the basis for the design in Fig. 1(*b*). In all, there are four internal feed channel types: the single channel without ribs, the single channel with ribs, the individual channels without ribs, and the individual channels with ribs.

Each internal channel design had three different cooling hole designs. The first had no cooling holes, the second had cylindrical holes, and the third had meter-diffuser-shaped holes. The meter-diffuser-shaped holes had 15 deg lateral expansion angles and a 1 deg forward expansion angle (15-15-1 holes). Both the cylindrical holes and 15-15-1 holes had injection angles of 30 deg. In both types of feed channels, ribs were discontinued near the inlet of the holes, as can be seen in Fig. 1. The location of the last rib before and the first rib after the cooling hole inlets is included in Table 1. For the Λ-shaped ribs, the location is based on the apex of the rib.

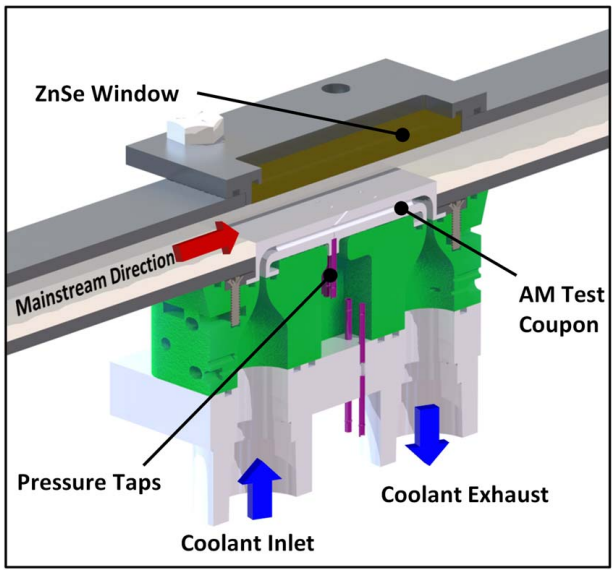

Fig. 2 Sectional view of the test section

Both types of cooling holes were designed to have the same engine scale metering diameter (D = 0.76 mm). The 15-15-1 holes also had inlet fillets with a radius (R) of $0.25D$. The film-cooling holes were staggered between two rows of holes for the individual channels. This staggering of the holes allowed for the spacing of the individual channels. The first row had five holes spaced $6D$ apart, and the second row of staggered holes had four holes also spaced $6D$ apart. The second row was $15D$ downstream of the first row. Note that only the individual channel coupons fed two rows of holes, as shown in Fig. 1(*b*), and the single channel fed only the first row, as shown in Fig. 1(*a*). The descriptors of the cylindrical holes and the 15-15-1 holes are summarized in Table 2.

The coupons were manufactured with the cooling holes oriented perpendicular to the substrate, which best practices have shown to reduce deviations from the design intent [37]. The parts were additively manufactured in Inconel 718 with a 40 μm layer height on an EOS M280, which is a direct metal laser sintering printer. Prior to removing the parts from the substrate, they were heat treated to remove residual stresses. Each coupon was computed tomography (CT) scanned to measure the relevant geometric parameters. An industrial CT scanner was used to get a voxel size of 20 μm. The software used to process the CT scans can determine the surface down to 1/10th the voxel size [38].

Overall, the feed channels and cooling holes are printed close to their design intents. The cooling hole minimum cross-sectional area deduced from the CT scan was used in the calculations of the blowing ratio. The cross-sectional area of the cooling holes ranged from <1% below the design intent to 12.4% larger than the design intent. Of all the cooling holes, only the cylindrical holes fed by the single channel without ribs were, on average, smaller than the design intent; the rest of the holes were slightly oversized. Although the vertical build direction is the optimal build orientation for minimal deviation from the design intent, small channels built vertically typically result in larger than intended with no adjustments for AM [37].

The average feed channel hydraulic diameter and cross-sectional area were used to set the internal Reynolds number. Because the cooling holes had an injection angle of 30 deg and were built perpendicular to the substrate, the feed channels were at a 60 deg angle to the substrate. A 60 deg build orientation creates surfaces close to the design intent with only a little more roughness than a surface built vertically [37]. The cross-sectional areas of the feed channels ranged from 1.7% below the design intent to 5.5% larger than the design intent. The average arithmetic mean roughness was found to be 9 μm on the downward-facing surfaces of the single channels. This arithmetic mean roughness indicates that the size of the AM roughness features was significantly smaller than the ribs.

4 Experimental Approach

Overall effectiveness measurements were obtained using the same 1x film-cooling test rig from Veley et al. [32]. Figure 2 shows a sectional view of the test section, which contains a mainstream channel, the test coupon, and an instrumented plenum. The plenum supplied gaseous nitrogen (N_2) while the mainstream flow was heated to achieve the desired coolant-to-mainstream density ratio (DR) of 1.2 at the exit of the film-cooling hole. The density of the coolant in the channel was larger than at the exit of the hole because of the high pressure in the coolant channels. The

Table 3 Rig operating conditions

Parameter	Value
Ma_∞	0.3
Ma_c	<0.1
$Re_{i,d}$	14,000
DR	1.2
M	≤3
Bi	0.2

operating conditions of the overall effectiveness tests are summarized in Table 3.

The mainstream air was heated to 50 °C and pressurized to 358 kPa with the flow rate measured upstream using a turbine flow meter. An upstream pressure regulator and a downstream butterfly valve were used to independently control the mainstream Reynolds number and Mach number. The mainstream Mach number (Ma_∞) was set at 0.3. The mainstream channel was 25.4 mm wide and 9.5 mm high (12.5 cooling hole diameters) and had more than 35 mainstream channel diameters before the test coupon to achieve hydrodynamically fully developed flow.

The internal channel mass flow rate was measured using a laminar flow element. Because part of the coolant flow is exhausted through the cooling holes, the flowrate upstream of the holes is higher than the flowrate downstream of the holes. For these studies, the downstream supply channel Reynolds number was maintained constant for each test ($Re_{i,d} = 14$ k). Maintaining $Re_{i,d}$ ensured that the supply channel's convective boundary condition remained the same for comparing the coupons. At $Re_{i,d} = 14$ k, the total mass flow rate through the single channel was only 1.1 times the total mass flow rate through all nine of the individual channels. The ratio of mass flow rates between channel types is directly related to the ratio of channel perimeters.

The mass flow rate through the film-cooling holes was set using the pressure ratio (PR) across the holes. A downstream valve for the internal channel supply was used to set the pressure ratio across the hole, which set the desired blowing ratio (M). The mass flow rate was set using a pressure ratio to flow parameter (FP) curve for each of the coupons. The PR was measured between the mainstream channel and pressure taps at the inlet of the holes, which can be seen in Fig. 2. For the rows at $X/D = 0$, there were pressure taps located across the supply channel from the inlet of the three center holes. For the second-row holes at $X/D = 15$, there were pressure taps that were additively printed at the inlets of the two center holes. For the coupons with two rows of holes, there was not a significant pressure drop between the first row of holes and the second row. The PR of the second row was within 5% of the PR of the first row. Consequently, the PR used was an average of the first and second rows, and the blowing ratio of both rows was approximately equal. As a result of the designs, the coupons with two rows of holes will have a greater mass flow rate through the surface than the coupons with a single row of holes for the same blowing ratio.

Separate experiments were conducted to obtain the PR to FP curves shown in Fig. 3. These experiments used a known mass flow rate through the holes and measured the pressure ratio. The data in Fig. 3 show that the hole shape has a greater influence on the FP than does the channel type or the ribs. Filleted inlets, such as those on the 15-15-1 holes, have been shown to increase the flow through a hole for a given PR [32,39]. At PR = 1.5, the 15-15-1 holes have an average FP 40% higher than cylindrical holes fed by the same channel type. Ribs, which have also been seen to affect the flow through film-cooling holes [40], had a small impact on the FP compared to the hole shape. At PR = 1.5, the presence of ribs decreased the FP through the 15-15-1 holes by an average of 11% and the cylindrical holes by an average of 6%. The channel shape had a minimal impact on FP.

To evaluate the Biot numbers for the coupons, the heat transfer coefficient on the mainstream side of the test coupon (h_∞) was

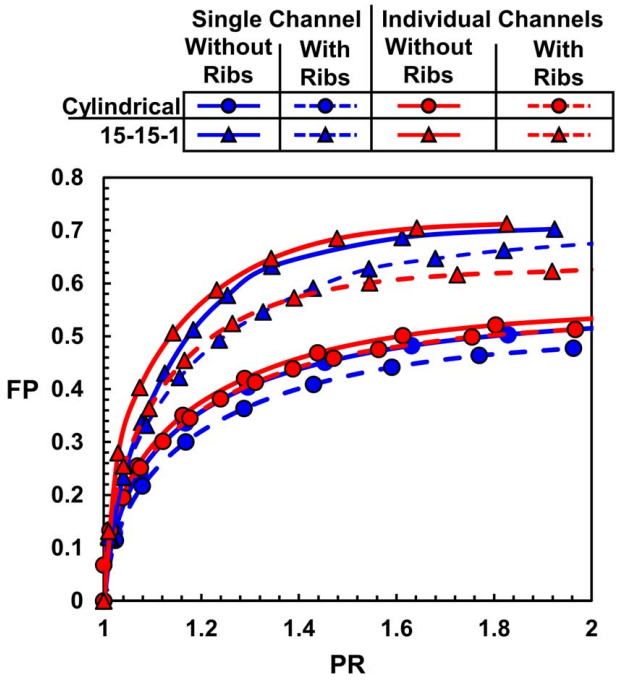

Fig. 3 The flow parameter as a function of pressure ratio for all coupons with cooling holes

calculated as a thermally developing boundary layer between two flat plates, with one side having a constant heat flux [41]. The correlation provided heat transfer coefficients within 35% of the h_∞ value estimated from the surface temperature and the mainstream temperature of the coupons without film cooling. Based on these calculations, the Biot number was estimated to be 0.2, which is within the estimated range of airfoil Biot numbers ($0.1 < Bi < 1$) [42]. From an energy balance between the external wall temperature and the coolant inlet and exit temperatures, the coupons without film-cooling holes were used to calculate the internal heat transfer coefficient (h_i) for each of the four internal channel types. The individual channels have a higher h_i than the single rectangular channel. Similarly, ribbed channels have higher h_i than the same type of channel without ribs. The ratio of external to internal convection coefficients (h_∞/h_i) at $Re_{i,d} = 14$ k is included in Table 4. The trends between channels of the h ratios are the inverse of the h_i relationships.

Tests were conducted to get the overall effectiveness (φ) of each test coupon at several blowing ratios, for which the test conditions are summarized in Table 3. The surface temperature of the coupon was measured using an infrered (IR) camera outside of the zinc solenoid window opposite the test coupon, which can be seen in Fig. 2. The IR camera was calibrated against surface thermocouples. The imaged surfaces of the test coupons were painted black to provide a high emissivity. For each test case, ten IR images were averaged together to reduce the precision uncertainty of the surface temperature. To calculate the overall effectiveness, the

Table 4 Parameters of channels without cooling holes

Channel	$S:V$ (m^{-1})	h_∞/h_i ($Re_i = 14$ k)	$\bar{\bar{\phi}}_0$ ($-5 \le X/D \le 10$)
Single channel			
No ribs	0.85:1	1.6	0.20
45 deg Λ-ribs	0.93:1	1.3	0.23
Individual channels			
No ribs	5.25:1	0.7	0.36
90 deg ribs	7.29:1	0.5	0.42

temperature at the inlet of the film-cooling holes (T_c) was also required. For all experiments, the overall cooling effectiveness was calculated using the temperature at the inlet of the first row of holes. This coolant temperature was calculated using an energy balance between the top wall temperature and the coolant channel. The upstream coolant mass low rate, the coolant inlet plenum temperature, h_i, and the surface temperature are known; therefore, the temperature at the inlet of the holes can be calculated. Another energy balance was conducted for the downstream region, and the calculated outlet temperature was found to be within 1.5 °C of the measured outlet plenum temperature for all test cases.

The absolute uncertainties were calculated using the propagation of uncertainties method [43]. The uncertainty of M is mainly dependent on the uncertainties of PR and FP. The uncertainty of M is 9.5%. The overall cooling effectiveness is dependent on the mainstream temperature (T_∞), the coolant temperature, and the surface temperature (T_s). The absolute uncertainty for φ is ± 0.02 at $\varphi = 0.25$. Repeatability testing was conducted for at least one blowing ratio with all eight coupons with film-cooling holes, with six of the eight coupons specifically repeated at $M = 1$. For the coupons without film-cooling holes, testing was also repeated at least once at $Re_i = 14$ k. All of the repeat φ results were within the uncertainty range of the original tests.

5 Computational Setup

Flow conjugate simulations were conducted for all geometries at a single-blowing ratio to show the effects of channel shape and ribs on the flow structure inside the cooling holes. STAR CCM+ [44] was used for the steady Reynolds-averaged Navier–Stokes (RANS) simulations with k-ω turbulence models. The domains of the simulations were three hole diameters wide. This domain was equivalent to half the coverage area of two holes, one in the first row and one in the second row. Because all the test cases were with symmetric geometries in co-flow, symmetry planes were incorporated at the center of the holes. For the Λ-rib single-channel cases, the center hole was simulated to make the symmetry boundary applicable.

A grid independence study was conducted for the geometry with cylindrical holes fed by individual channels without ribs. Three meshes were tested: 4.3 million cells, 6.3 million cells, and 7.8 million cells. Between the 6.3-million and 7.8-million cell simulations, the lateral averaged overall effectiveness differed less than 0.01 for any given streamwise location. The 6.3-million cell mesh was therefore selected for use during the simulations. While validating the grid independence, the $y+$ values were also verified to be approximately 1 through the use of prism layers.

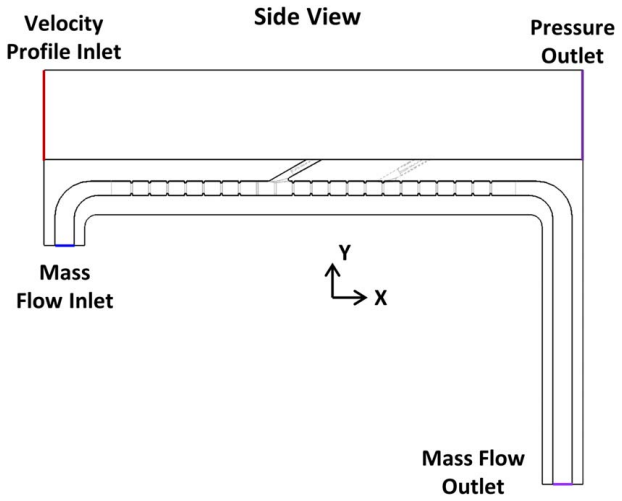

Fig. 4 Example of the CFD domain with the 15-15-1 holes fed by ribbed individual feed channels

The location of the boundary conditions can be seen in the diagram of the domain shown in Fig. 4. The velocity profile of the mainstream inlet was created through a two-dimensional simulation of the upstream section of the experimental test rig. The mass flow outlet was set to an internal Reynolds number of 14 k, while the coolant inlet mass flow was set as the sum of the mass flow through the cooling holes and the mass flow through the coolant outlet. As a conjugate simulation, the wall was given the material properties of Inconel 718 with a thermal conductivity of 9.77 W/m · K, which was measured in-house on an additively manufactured Inconel 718 test specimen.

6 Effect of Channel Type

The data in Fig. 5 show lateral averages of experimental baseline effectiveness with no film cooling (φ_0) as a function of streamwise location for all four internal channel geometries. All lateral averages reported in this paper are averaged over the range $-9 \le S/D \le 9$, which is the coverage area of the center three first-row holes. The effect of ribs on φ_0 will be discussed in the next section. As such, the first noticeable result for the non-ribbed coupons in Fig. 5 is that the coupon with individual channels had higher effectiveness than the single channel. The individual channels benefit from the added convective surface area that the walls in between channels provide, which the single channel does not have. Examining the ratios in Table 4, the surface area to flow volume ratio for the individual channels is approximately 6 times larger than the ratio for the single channels. Recall that the h_∞/h_i, also from Table 4, shows that the single channel h_∞/h_i is 2.3 times greater than the individual channels, indicating that the internal convection of the individual channels is superior to that of the single channel. However, it can be assumed that the pressure drop would be far larger across the individual feed channels than across the single channel, but this pressure drop measurement was beyond the scope of this paper.

Figures 6(*a*)–6(*d*) show overall effectiveness contours for both types of cooling holes at $M = 1$ fed by both types of non-ribbed supply channels. The contours of the holes fed by individual channels, shown in Figs. 6(*b*) and 6(*d*), have a higher overall effectiveness than the single channel, shown in Figs. 6(*a*) and 6(*c*). Therefore, the channel type has a greater impact on overall effectiveness than the addition of film cooling.

Although the channel type has a greater impact on overall effectiveness, the hole type has a small impact on the region of local high

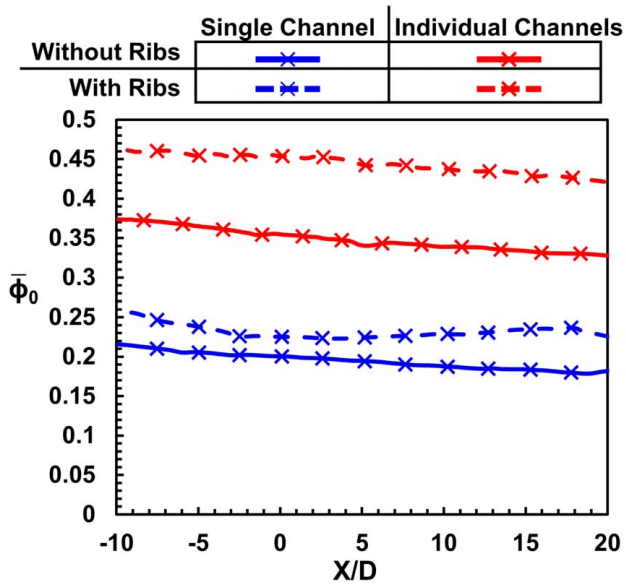

Fig. 5 Lateral average of the experimental baseline effectiveness for both channel types both including and not including ribs

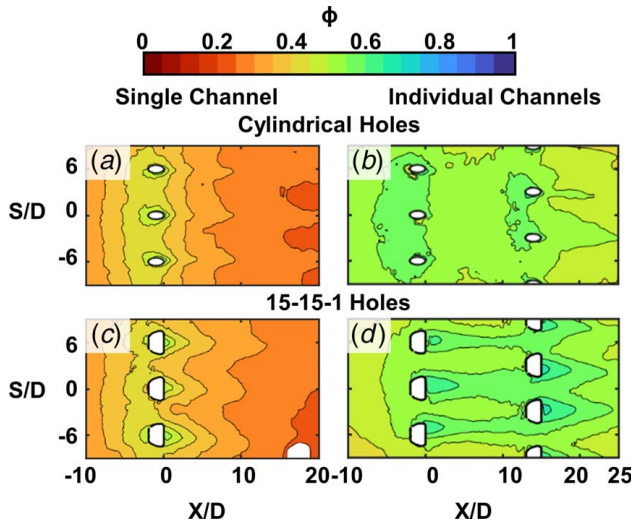

Fig. 6 Contours of overall effectiveness for (*a*) the cylindrical holes fed by the non-ribbed single channel, (*b*) the cylindrical holes fed by the non-ribbed individual channels, (c) the 15-15-1 holes fed by the non-ribbed single channels, and (*d*) the 15-15-1 holes fed by the non-ribbed individual channels at $M = 1$

effectiveness. For example, holes without inlet fillets and smaller diffuser angles have been seen to have a higher near-hole effectiveness ($X/D \leq 0$) than holes with inlet fillets [32]. Consequently, in the four overall effectiveness contours of Fig. 6, the cylindrical holes have a higher near-hole effectiveness than the 15-15-1 holes, which is especially noticeable between the hole outlets ($-2 \leq X/D \leq 0$). The 15-15-1 holes, however, can be seen in Figs. 6(*c*) and 6(*d*) to have greater lateral spreading of the cooling jet than the cylindrical holes. In fact, the contours in Fig. 6(*b*) indicate that the jets from the cylindrical holes fed by individual channels are fully detached. This detachment is corroborated by the centerline-hole velocity contours in Fig. 7(*a*) from the computational fluid dynamics (CFD) for the cylindrical holes fed by individual channels at $M = 1$, which depicts a region of separation downstream of the cylindrical hole outlet ($0 \leq X/D \leq 2$, $0 \leq Y/D \leq 1$). The cooling jet in Fig. 7(*a*) has separated, which is detrimental to the film-cooling performance because the coolant is not on the surface it is intended to cool.

The impacts of the blowing ratio on overall effectiveness are shown in Fig. 8 of all geometries across the range of blowing ratios. The region averaged was $-9 \leq S/D \leq 9$ and $-5 \leq X/D \leq 10$, which is the coverage area of the center three first-row holes, and only extends to the start of the second row of holes for the cases that have a second row. To show the area-average trend of the baselines, ϕ_0 was included for $M = 0$. These first-row area averages are also included in Table 4. The individual channels have a ϕ_0 that is 80% higher than that of the single channel. In fact, the results in Fig. 8 show that in order to obtain an overall effectiveness equivalent to the baseline effectiveness on the non-ribbed individual channels without film cooling, the non-ribbed single channel has to pass enough coolant through the cooling holes to set $M = 1$ ($\phi_{15-15-1} = 0.36$). Therefore, the same effectiveness can be obtained from a supply channel with superior cooling performance but without film cooling as can be obtained from a supply channel with poor internal cooling performance that has the added benefit of film cooling.

To assess the augmentation of the film-cooling, the data are presented in Fig. 9 for an $M = 1$ as a difference relative to the non-film-cooled surface normalized by the non-film-cooled surface. The streamwise range ($-10 \leq X/D \leq 20$) included in Fig. 9 incorporates the region ($-10 \leq X/D \leq 10$) most effected by the common row of cooling holes between channel types. The data in Fig. 9 show that the film-cooling augmentation is higher for the single-channel-fed first row of holes than for the individual-channel-fed first row of holes. The single channels have a higher film-cooling augmentation than the individual channels because the single channel has a low baseline effectiveness. Therefore, any amount of film cooling is highly beneficial for the single channel.

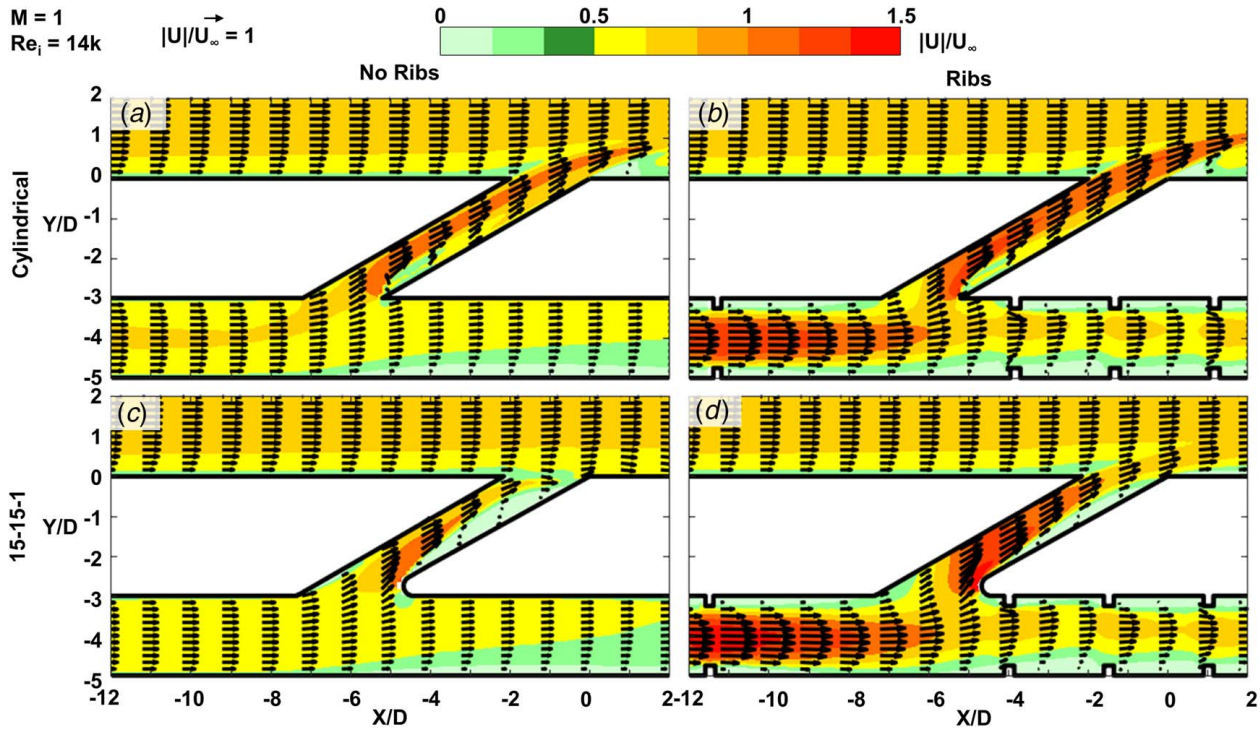

Fig. 7 Velocity magnitude contours and velocity vectors on the first-row hole's centerline plane at $M = 1$ predicted by CFD of (*a*) a cylindrical hole fed by a non-ribbed individual channel, (*b*) a cylindrical hole fed by a ribbed individual channel, (c) a 15-15-1 hole fed by a non-ribbed individual channel, and (*d*) a 15-15-1 hole fed by a ribbed individual channel

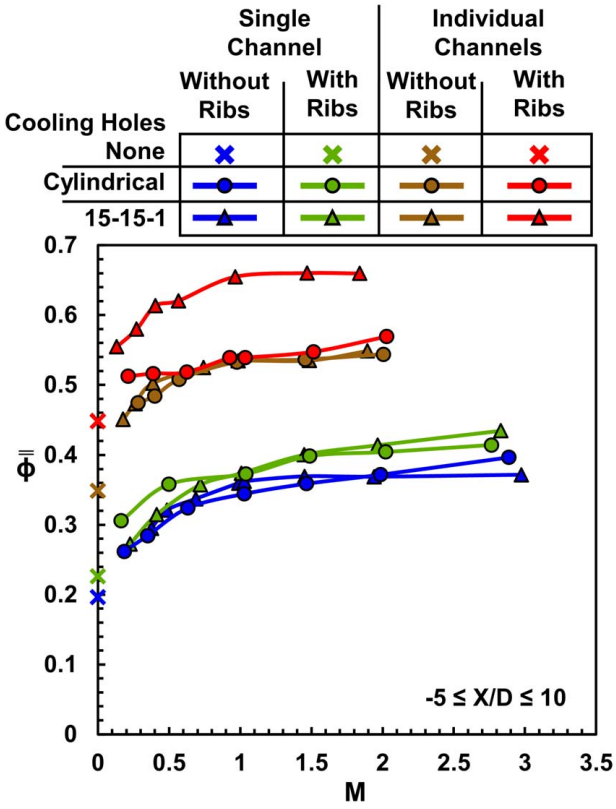

Fig. 8 Area-averaged overall cooling effectiveness across several blowing ratios of the first row of holes ($-5 \le X/D \le 10$) for all geometries

The data for the individual channels show a relatively constant augmentation in the streamwise direction relative to the single channel, as shown in Fig. 9. These constant augmentation levels for the individual channels are a result of the high convective heat transfer resulting from the small internal channels in the streamwise direction. Conversely, the single-channel supply feed is subject to the upstream convection of the holes and the downstream diffusion of the film cooling, as indicated by the changing augmentation values.

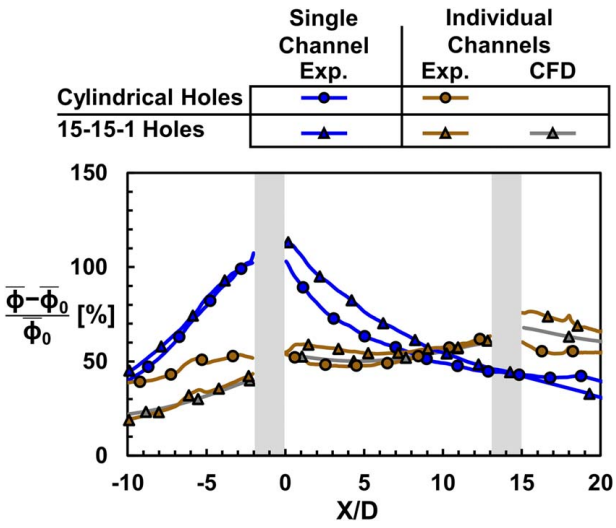

Fig. 9 Lateral averages of film-cooling augmentation for the non-ribbed coupons and for the numerical simulation of the 15-15-1 hole fed by non-ribbed circular individual channels at $M = 1$

The film-cooling augmentation from the CFD predictions of the 15-15-1 holes fed by individual channels is also included in Fig. 9. The RANS predictions have a relatively good comparison from a lateral average perspective with the measurements. Although RANS simulations typically miss-predict the mixing and decay of film-cooling [45] on an adiabatic boundary condition, the conduction included in the conjugate heat transfer prediction results has relatively good agreement with the experiments.

The CFD flow field results in Figs. 10(*a*)–10(*h*) show the velocity contours of the flow normal to the breakout plane overlaid with the in-plane flow vectors for all the geometries at $M = 1$. The flow through the cylindrical holes fed by a non-ribbed single channel, seen in Fig. 10(*a*), shows the common rotating vortex pair that has been previously reported [46]. Conversely, the flow in the cylindrical hole fed by an individual channel, shown in Fig. 10(*e*), results in a different in-plane flow pattern with two vortex pairs (instead of only one pair) and a peak velocity closer to the windward side of the hole at the breakout location on the main gas path side. Because of the relatively high velocity ($U_{hole}/U_\infty > 1$) in the cylindrical holes, the jets have a greater momentum than the external flow causing the jets to lift off, as seen in Fig. 7(*a*), which is deleterious to the film-cooling effectiveness. The effects of the liftoff can be seen in the experimental results as the high decay in effectiveness immediately downstream of the hole exit ($0 \le X/D < 3$), as shown in the overall effectiveness contours of Figs. 6(*a*) and 6(*b*) and the film-cooling augmentation lateral averages of Fig. 9.

The flow fields for the 15-15-1 holes fed by the two different non-ribbed channels are shown in Fig. 10(*c*) (non-ribbed single channel) and Fig. 10(*g*) (non-ribbed individual channel). Figures 10(*c*) and 10(*g*) show that the highest velocities for both channel types are at the windward side of the hole where the coolant spreads

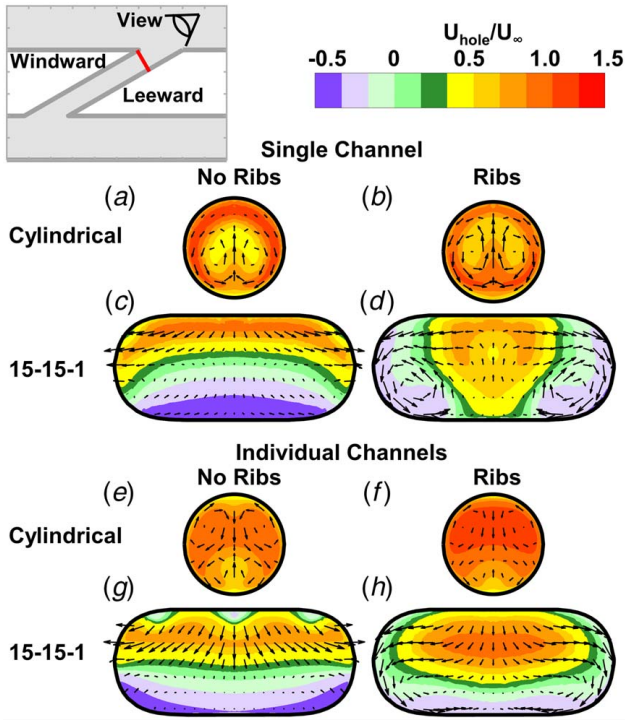

Fig. 10 Contours at $M = 1$ of normalized velocity normal to the first-row hole breakout plane and the in-plane flow vectors for (*a*) cylindrical hole fed by non-ribbed single channel, (*b*) cylindrical hole fed by Λ-ribbed single channel, (c) 15-15-1 hole fed by non-ribbed single channel, (*d*) 15-15-1 hole fed by Λ-ribbed single channel, (e) cylindrical hole fed by non-ribbed individual channel, (*f*) cylindrical hole fed by ribbed individual channel, (*g*) 15-15-1 hole fed by non-ribbed individual channel, and (*h*) 15-15-1 hole fed by ribbed individual channel (the windward side of the hole is on top and the leeward side is on the bottom)

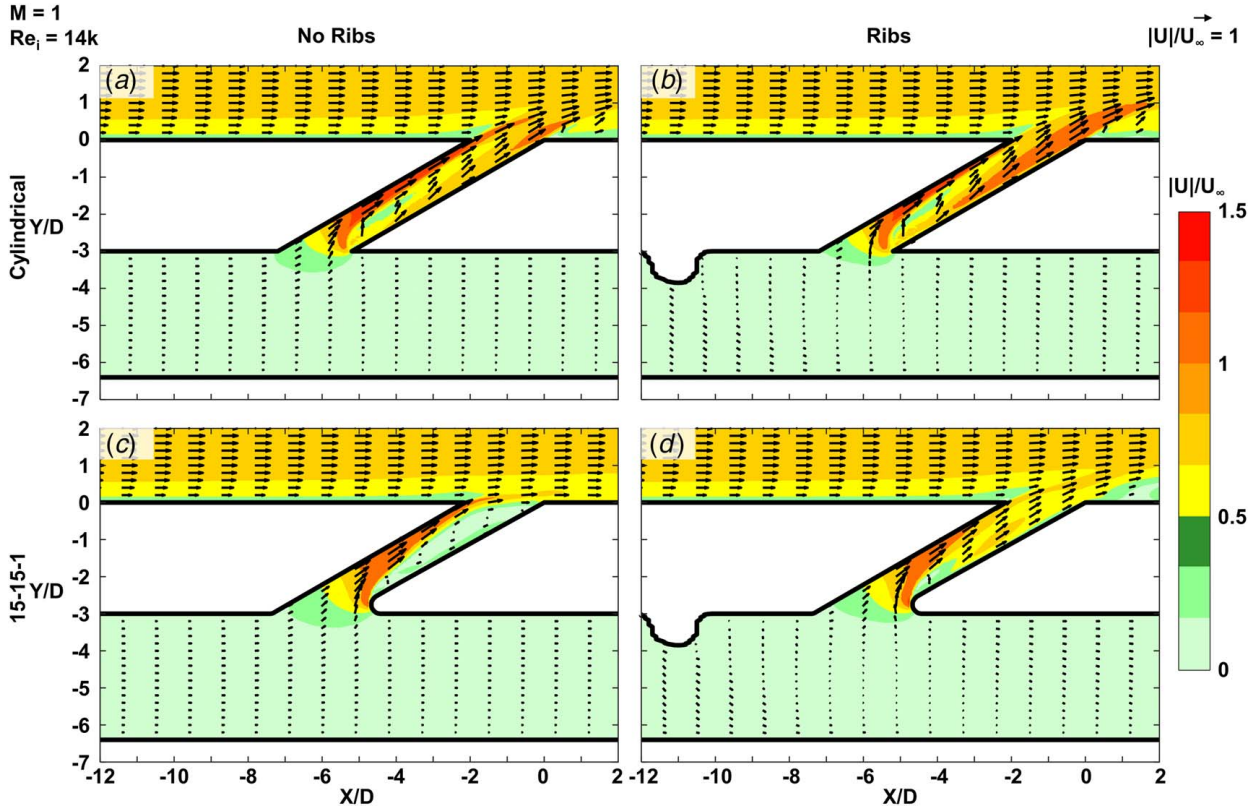

Fig. 11 Velocity magnitude contours and velocity vectors on the first-row hole's centerline plane at $M = 1$ predicted by CFD of (*a*) a cylindrical hole fed by a non-ribbed single channel, (*b*) a cylindrical hole fed by a Λ-ribbed single channel, (c) a 15-15-1 hole fed by a non-ribbed single channel, and (*d*) a 15-15-1 hole fed by a Λ-ribbed single channel

outward as the hole diffuses. Similarly, at the leeward side of both holes, there is a recirculation region with low levels of reverse flow. This recirculation region within the diffuser of the 15-15-1 holes can be seen in the center plane velocity contours of Fig. 7(*c*) (individual channel) and Fig. 11(*c*) (single channel). The combination of these internal flow structures allows the coolant to remain closer to the wall, as seen in the velocity plot of Fig. 7(*c*), giving the 15-15-1 hole a slight improvement in film-cooling augmentation over the cylindrical holes, as shown in the contours of Fig. 6 and the lateral averages of Fig. 9.

7 Effect of Ribs

Ribs in the supply channels increase the overall effectiveness, which is shown in Fig. 5, by increasing the internal convection. The lateral averages of $\phi 0$ for all four internal designs, shown in Fig. 5, illustrate that the ribbed channels have a higher baseline effectiveness than the corresponding non-ribbed supply. Ribs both increase the flow turbulence and increase the surface area to flow volume ratio, which is listed in Table 4. For the single-channel feed, the Λ-ribs increase the surface area by 4% and create vortex structures that increase internal heat transfer, resulting in a ribbed ϕ_0 that is 22% higher than the baseline of the non-ribbed single channel. For the individual channels, the ribs increase the surface area by 10% and induce secondary flows, resulting in a ribbed ϕ_0 that is 29% higher than the baseline of the non-ribbed individual channel. The addition of ribs increased the internal convective coefficient, showing that ϕ_0 is inversely related to the h_∞/h_i reported earlier. This relationship between φ_0 and h_∞/h_i is consistent with the one-dimensional analysis presented by Williams et al. [47], who used the one-dimensional analysis to introduce the equation

$$\phi_0 = \frac{1}{1 + \mathrm{Bi} + (h_\infty/h_i)} \quad (1)$$

As expected for the rib channels, Fig. 8 indicates that the overall effectiveness increases with increasing blowing ratio. Of the four ribbed channel designs, the cylindrical holes fed by ribbed individual channels were the least sensitive to the blowing ratio. In fact, in Fig. 8, the overall effectiveness of the cylindrical holes fed by ribbed individual channels is about the same between the ribbed and non-ribbed channels for $M \geq 0.6$. The suspected reason for the relatively low film-cooling augmentation of the cylindrical holes fed by the ribbed individual channels is the high relative velocity within the hole, which can be seen in Fig. 10(*f*) for $M = 1$. The relatively high velocity within the hole does not match the momentum or direction of the mainstream boundary layer. At the operating conditions described in Table 3, there are local Mach effects within the cooling holes [32] that result in variations of the local density and consequently of the local momentum. The cooling jet, therefore, penetrates past the mainstream boundary layer, as seen in the CFD velocity contours in Fig. 7(*b*). Recall that for the individual channels, the last rib before the hole is located at $X/D = -11.7$, and the first rib after the hole inlet is located at $X/D = -3.7$, as can be seen in Figs. 7(*b*) and 7(*d*).

The centerline-hole velocity contours in Figs. 11(*a*) and 11(*b*) of the cylindrical holes fed by the single channel show that the flow through the holes does not significantly change in regions of very low velocity (green contours) within the hole. However, throughout the majority of the hole, the region of high velocity in the non-ribbed case was on the windward side of the hole, as seen in Fig. 11(*a*), but the region of high velocity in the Λ-ribbed case was on the leeward side of the hole, as seen in Fig. 11(*b*). Similarly, the vortical structure caused by the ribs in the individual channels moves the high-speed region to the leeward side to the cylindrical hole, seen in the breakout plane in Fig. 10(*b*), compared to the non-ribbed case seen in the breakout plane in Fig. 10(*a*). Likewise, for the 15-15-1 holes, the Λ-ribs in the single channel cause the cooling jet to not fully diffuse at $M = 1$, as seen in Fig. 10(*d*), and

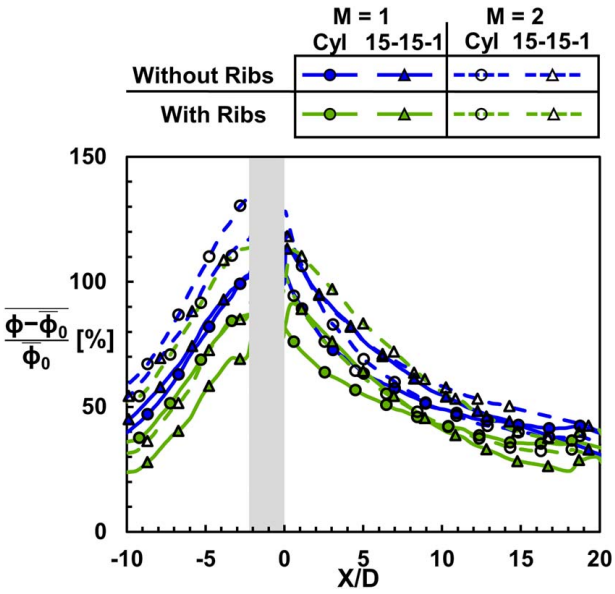

Fig. 12 Lateral average of film-cooling augmentation at $M = 1$ & 2 for holes fed by non-ribbed and ribbed single channels

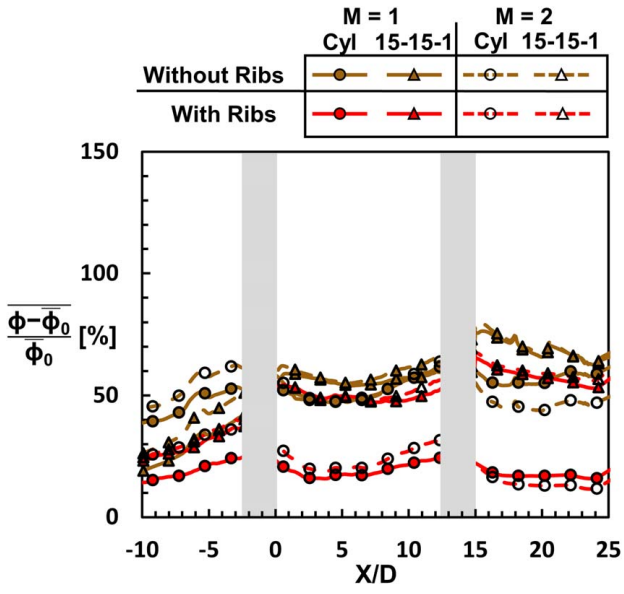

Fig. 13 Lateral average of film-cooling augmentation at $M = 1$ & 2 for holes fed by non-ribbed and ribbed individual channels

the jet detaches, as seen in Fig. 11(*d*). Recall that the single channel has the apex of the last Λ-rib located before the hole at $X/D = -11$ and the first after the hole inlet at $X/D = 14.5$, which is outside the streamwise range shown in Figs. 11(*b*) and 11(*d*).

Figure 12 shows the lateral average of film-cooling augmentation for both types of holes fed by single channels. Consistent with the area-average results, increasing the blowing ratio increases the film-cooling augmentation, which is exemplified by the fact that at $M = 2$, each geometry has the same or a higher film-cooling augmentation than it has at $M = 1$.

Although the overall effectiveness was higher for the ribbed channels compared to the non-ribbed channels, the data in Fig. 12 show that the augmentation is generally lower for the ribbed channels, which is a result of already high internal convective heat transfer for the ribbed cases. The only case where the ribbed channel has approximately the same or higher film-cooling augmentation than the corresponding non-ribbed channel is that of the 15-15-1 hole at $M = 2$. The 15-15-1 holes fed by the non-ribbed single channel had a difference in film-cooling augmentation between the $M = 1$ and $M = 2$ cases that were less than the experimental uncertainty, whereas the corresponding ribbed cases had an experimentally significant increase in film-cooling augmentation along the entire downstream section ($X/D > 0$). The suspected reason that 15-15-1 holes fed by the non-ribbed single channel have similar film-cooling augmentation at the two blowing ratios is that the jet is attached at $M = 1$, which can be seen in the center plane velocity plot in Fig. 11(*c*) and the overall effectiveness contours in Figs. 6(*c*) and 6(*d*), but the added coolant in the cooling jet for $M = 2$ potentially causes the jet to slightly detach. However, with the Λ-ribs, the flow through the 15-15-1 hole did not fully diffuse, as shown in Fig. 10(*d*). At the center plane shown in Fig. 11(*d*), the flow does not have the large recirculation zone in the diffuser like the non-ribbed case shown in Fig. 11(*c*) but has fairly uniform velocity through the hole in this plane.

The lateral average film-cooling augmentation results at $M = 1$ and $M = 2$ for the individual channels are in Fig. 13. Note that the film-cooling augmentation range presented on the *y*-axis was maintained from Fig. 12, thereby showing that the film-cooling augmentation results in Fig. 13 do not reach the high augmentation (near 100%) for either row of the individual-channel-fed holes as occurred for the single-channel-fed holes shown in Fig. 12, which is a function of the high $\phi 0$ for the individual channels. The lower film-cooling augmentation for the individual channels is consistent with the non-ribbed channel results at $M = 1$ in Fig. 9.

The lateral averages in Fig. 13 indicate that increasing the blowing ratio does not guarantee an increase in film-cooling augmentation for both rows of holes. For the cylindrical holes, the second row of holes ($X/D \geq 15$) has about the same lateral average film-cooling augmentation at $M = 1$ and $M = 2$. The reason is that at both $M = 1$ and $M = 2$, the jet fully separates from the surface at both rows of holes, as indicated by the lateral averages in Fig. 13. Because the coolant from neither row of holes remains well within the film on the surface, downstream of the second row receives only marginal benefits from film cooling from either row. Consequently, the film-cooling augmentation is significantly less for the cylindrical holes fed by ribbed individual channels than for any other geometry at either blowing ratio.

For the 15-15-1 holes, the downstream ($X/D \geq 0$) film-cooling augmentation in Fig. 13 is approximately equivalent between the two blowing ratios for both rows of holes regardless of the presence of rib or not. Similar to the Λ-ribs in the single channel causing the flow through the 15-15-1 hole to not fully diffuse, which is seen in Fig. 10(*d*), the ribs in the individual channels also cause the coolant to not fully diffuse in the 15-15-1 hole, which can be seen in Fig. 10(*h*). Conversely, unlike the detached flow seen in Fig. 11(*d*) for the 15-15-1 holes fed by Λ-ribbed single channels, when the 15-15-1 hole is fed by ribbed individual channels, the coolant jet velocity closely matches the mainstream velocity and turns to the mainstream direction, thereby staying near the surface, as seen in Fig. 7(*d*).

The ribs not only affect the flow through the holes but also the flow in the supply channels. For example, the non-ribbed individual channels have a high-velocity flow biased toward the film-cooled wall side of the internal channel after the hole ($X/D > -4$, $Y/D < -3$), as shown in Figs. 7(*a*) and 7(*c*). The ribbed individual channels also experience a bias immediately after the hole in the internal flow, but the downstream ribs trip the flow, thereby mitigating the bias of the high-velocity flow, as can be seen in Figs. 7(*b*) and 7(*d*). The skewed flow toward the film-cooled wall in the non-ribbed channels did not offset the benefit that the ribs provided for the overall effectiveness.

8 Conclusions

This paper covered experimental and computational results on the effects of feed channels and ribs. Experiments used additively manufactured cooling holes at the engine scale with a matched Biot number. The geometries included cylindrical holes and 15-15-1 holes fed by one of four different supply channel types: a single rectangular channel, a single rectangular channel with Λ-shaped ribs, nine circular individual feed channels, or nine circular individual feed channels with ribs. The single channels had a single row of holes, and the individual channels had two rows of holes where each channel fed one cooling hole.

The individual channels were seen to have a higher baseline overall cooling effectiveness without any film cooling than the single channel without film cooling. Similarly, for both the single channel and the individual channels, the addition of ribs increased the baseline effectiveness. The ribbed individual channels had a higher baseline effectiveness than any of the single channels with film cooling. Therefore, it can be concluded that the internal cooling scheme is very important to the overall component cooling. Because the individual channels had a higher baseline effectiveness, the film-cooling augmentation was lower for the individual channels than it was for the single channels. However, the second row of holes caused the film-cooling augmentation of the individual channels to be less sensitive to the streamwise location than the single channels.

The channel type and ribs affected the velocity field. Both channel shape and ribs affected the flow structure in the cooling holes. The presence of ribs had a greater impact on the flow through the 15-15-1 holes than on the flow through the cylindrical ribs. Without ribs, the flow stays attached to the lateral diffuser walls of the 15-15-1 holes, whereas with ribs, the secondary flows cause more rotation within the holes, which leads to jet detachment.

In all, the overall effectiveness is heavily dependent on the internal feed channel design; therefore, much consideration should be given to this part when regarding designs.

Acknowledgment

This paper is based upon work supported by the Department of Energy under Award Number DE-FE0025011. This report was prepared as an account of work sponsored by an agency of the United States Government. Neither the United States Government nor any agency thereof, nor any of their employees, makes any warranty, express or implied, or assumes any legal liability or responsibility for the accuracy, completeness, or usefulness of any information, apparatus, product, or process disclosed, or represents that its use would not infringe privately owned rights. Reference herein to any specific commercial product, process, or service by trade name, trademark, manufacturer, or otherwise does not necessarily constitute or imply its endorsement, recommendation, or favoring by the United States Government or any agency thereof. The views and opinions of authors expressed herein do not necessarily state or reflect those of the United States Government or any agency thereof.

Conflict of Interest

There are no conflicts of interest.

Data Availability Statement

The datasets generated and supporting the findings of this article are obtainable from the corresponding author upon reasonable request.

Nomenclature

e = rib height
h = convective heat transfer coefficient
k = thermal conductivity
p = perimeter
t = hole breakout width
D = film-cooling hole metering diameter
H = channel height
L = cooling hole length
M = blowing ratio, $(\dot{m}_f/A_{min})/(\rho_\infty U_\infty)$
P = pitch spacing
R = fillet radius
S = spanwise coordinate
T = temperature
U = local velocity
V = mass average velocity
X = streamwise coordinate
Y = vertical coordinate
$\dot{m}$ = mass flow rate
t_{wall} = coupon wall thickness
A_c = cross-sectional flow area
A_{min} = minimum cross-sectional area of cooling hole meter
D_h = hydraulic diameter, $4A_c/p$
P_c = pressure in coolant channel at hole inlet
U_∞ = maximum/centerline velocity
Bi = Biot number, $h_\infty t_{wall}/k_\infty$
DR = density ratio, ρ_c/ρ_∞
FP = mass flow parameter, $\dot{m}(RT_c)^{0.5}/P_c A_c$
PR = pressure ratio
Re = Reynolds number, $(4\dot{m})/(p\mu)$
S:V = surface area to volume ratio

Greek Symbols

μ = dynamic viscosity
ρ = fluid density
ϕ = overall effectiveness, $(T_\infty - T_s)/(T_\infty - T_c)$
$\overline{\phi}_0$ = laterally averaged overall effectiveness
$\underline{\phi}$ = area-averaged overall effectiveness
ϕ_0 = overall effectiveness without film cooling

Subscripts

c = coolant
d = downstream of holes
f = film
hole = hole normal direction
i = coupon internal channel
m = metering section
s = coupon surface
∞ = mainstream

References

[1] Thole, K. A., Gritsch, M., Schulz, A., and Wittig, S., 1997, "Effect of a Crossflow at the Entrance to a Film-Cooling Hole," ASME J. Fluids Eng., **119**(3), pp. 533–540.
[2] Wilfert, G., and Wolff, S., 1999, "Influence of Internal Flow on Film Cooling Effectiveness," ASME J. Turbomach, **122**(2), pp. 327–333.
[3] Kohli, A., and Thole, K. A., 1998, "Entrance Effects on Diffused Film-Cooling Holes," International Gas Turbine and Aeroengine Congress and Exhibition, Stockholm, Sweden.
[4] Brundage, A. L., Plesniak, M. W., and Ramadhyani, S., 1999, "Influence of Coolant Feed Direction and Hole Length on Film Cooling Jet Velocity Profiles," International Gas Turbine and Aeroengine Congress and Exhibition, Indianapolis, IN.
[5] Fox, D. W., Jones, F. B., McClintic, J. W., Bogard, D. G., Dyson, T. E., and Webster, Z. D., 2019, "Rib Turbulator Effects on Crossflow-Fed Shaped Film Cooling Holes," ASME J. Turbomach., **141**(3), p. 031013.
[6] Sakai, E., Takahashi, T., and Agata, Y., 2013, "Experimental Study on Effects of Internal Ribs and Rear Bumps on Film Cooling Effectiveness," ASME J. Turbomach., **135**(3), p. 031025.

[7] Peterson, S. D., and Plesniak, M. W., 2002, "Short-Hole Jet-in-Crossflow Velocity Field and Its Relationship to Film-Cooling Performance," Exp. Fluids, **33**(6), pp. 889–898.
[8] Stimpson, C. K., Snyder, J. C., Thole, K. A., and Mongillo, D., 2018, "Effects of Coolant Feed Direction on Additively Manufactured Film Cooling Holes," ASME J. Turbomach., **140**(11), p. 111001.
[9] Hale, C. A., Plesniak, M. W., and Ramadhyani, S., 2000, "Film Cooling Effectiveness for Short Film Cooling Holes Fed by a Narrow Plenum," ASME J. Turbomach., **122**(3), pp. 553–557.
[10] Lerch, A., Schiffer, H. P., and Klaubert, D., 2011, "Impact on Adiabatic Film Cooling Effectiveness Using Internal Cyclone Cooling," Turbo Expo: Power for Land, Sea, and Air, Vancouver, British Columbia, Canada.
[11] McClintic, J. W., Anderson, J. B., Bogard, D. G., Dyson, T. E., and Webster, Z. D., 2018, "Effect of Internal Crossflow Velocity on Filsm Cooling Effectiveness-Part I: Axial Shaped Holes," ASME J. Turbomach., **140**(1), p. 011003.
[12] Zhu, R., Li, S., and Xie, G., 2022, "Conjugate Heat Transfer and Flow Features of Single-Hole and Combined-Hole Film Cooling With Rib-Roughened Internal Passages," ASME J. Therm. Sci. Eng. Appl., **14**(9), p. 091006.
[13] Walters, D. K., and Leylek, J. H., 2000, "A Detailed Analysis of Film-Cooling Physics: Part I—Streamwise Injection With Cylindrical Holes," ASME J. Turbomach., **122**(1), pp. 102–112.
[14] Hyams, D. G., and Leylek, J. H., 2000, "A Detailed Analysis of Film Cooling Physics: Part III—Streamwise Injection With Shaped Holes," ASME J. Turbomach., **122**(1), pp. 122–132.
[15] Stimpson, C. K., Snyder, J. C., Thole, K. A., and Mongillo, D., 2018, "Effectiveness Measurements of Additively Manufactured Film Cooling Holes," ASME J. Turbomach., **140**(1), p. 011009.
[16] Li, C., An, B., and Liu, J., 2022, "Effect of Coolant Crossflow on Film Cooling Effectiveness of Diffusion Slot Hole With and Without Ribs," ASME J. Turbomach., **144**(9), p. 091005.
[17] Han, J. C., Zhang, Y. M., and Lee, C. P., 1991, "Augmented Heat Transfer in Square Channels With Parallel, Crossed, and V-Shaped Angled Ribs," ASME J. Heat Transfer, **113**(3), pp. 590–596.
[18] Han, J. C., and Zhang, Y. M., 1992, "High Performance Heat Transfer Ducts With Parallel Broken and V-Shaped Broken Ribs," Int. J. Heat Mass Transfer, **35**(2), pp. 513–523.
[19] Taslim, M. E., Li, T., and Kercher, D. M., 1996, "Experimental Heat Transfer and Friction in Channels Roughened With Angled, V-Shaped, and Discrete Ribs on Two Opposite Walls," ASME J. Turbomach., **118**(1), pp. 20–28.
[20] Kissel, H. P., Weigand, B., von Wolfersdorf, J., Numann, S. O., and Ungewickell, A., 2007, "An Experimental and Numerical Investigation of the Effect of Cooling Channel Crossflow on Film Cooling Performance," Turbo Expo: Power for Land, Sea, and Air, Montreal, Canada.
[21] Sakai, E., and Takahashi, T., 2011, "Experimental and Numerical Study on Effects of Turbulence Promoters on Flat Plate Film Cooling," Turbo Expo: Power for Land, Sea, and Air, Vancouver, British Columbia, Canada.
[22] Shen, J. R., Wang, Z., Ireland, P. T., Jones, T. V., and Byerley, A. R., 1996, "Heat Transfer Enhancement Within a Turbine Blade Cooling Passage Using Ribs and Combinations of Ribs With Film Cooling Holes," ASME J. Turbomach., **118**(3), pp. 428–434.
[23] Casarsa, L., and Arts, T., 2005, "Experimental Investigation of the Aerothermal Performance of a High Blockage Rib-Roughened Cooling Channel," ASME J. Turbomach., **127**(3), pp. 580–588.
[24] Cukurel, B., Selcan, C., and Arts, T., 2018, "Film Cooling Extraction Effects on the Aero-Thermal Characteristics of Rib Roughened Cooling Channel Flow," ASME J. Turbomach., **140**(8), p. 021016.
[25] Böttger, M., Lange, M., Mailach, R., and Vogeler, K., 2020, "Experimental Study on the Influence of Film Cooling Hole Extraction on Heat Transfer and Flow Field in Internal Ribbed Cooling Channels of Turbine Blades," ASME J. Turbomach., **142**(10), p. 101005.
[26] Agata, Y., Takahashi, T., Sakai, E., and Nishino, K., 2013, "Effect of Orientation of Internal Turbulence Promoting Ribs on Flow Characteristics for Film Cooling," J. Therm. Sci. Technol., **8**(1), pp. 15–27.
[27] Klavetter, S. R., McClintic, J. W., Bogard, D. G., Dees, J. E., Laskowski, G. M., and Briggs, R., 2016, "The Effect of Rib Turbulators on Film Cooling Effectiveness of Round Compound Angle Holes Fed by an Internal Cross-Flow," ASME J. Turbomach., **138**(12), p. 121006.
[28] Lu, B., Peng, W., Jiang, P. X., Wang, J., and Wang, Y. P., 2017, "Experimental and Numerical Study of the Effect of Conjugate Heat Transfer on Film Cooling," Exp. Heat Transfer, **30**(4), pp. 355–368.
[29] Wang, J., Gu, C., and Sunden, B. A., 2015, "Conjugated Heat Transfer Analysis of a Film Cooling Passage With Different Rib Configurations," Int. J. Numer. Methods Heat Fluid Flow, **25**(4), pp. 841–860.
[30] Krille, T., Poser, R., von Wolfersdorf, J., and Henze, M., 2023, "An Experimental Investigation on Pressure Loss and Local Heat Transfer Characteristics in Additively Manufactured Ribbed Cooling Configurations," Int. J. Heat Mass Transfer, **202**, p. 123668.
[31] Snyder, J. C., and Thole, K. A., 2020, "Performance of Public Film Cooling Geometries Produced Through Additive Manufacturing," ASME J. Turbomach., **142**(5), p. 051009.
[32] Veley, E. M., Thole, K. A., Furgeson, M. T., and Bogard, D. G., 2023, "Printability and Overall Cooling Performance of Additively Manufactured Holes With Inlet and Exit Rounding," ASME J. Turbomach., **145**(3), p. 031017.
[33] Gutierrez, D., Yoon, C., Furgeson, M. T., Veley, E. M., Bogard, D. G., and Thole, K. A., 2022, "Evaluation of Adjoint Optimized Hole—Part I Baseline Performance," ASME J. Turbomach.
[34] Jones, F. B., Fox, D. W., Oliver, T., and Bogard, D. G., 2021, "Parametric Optimization of Film Cooling Hole Geometry," Turbo Expo: Power for Land, Sea, and Air, Virtual, Online.
[35] Rallabandi, A. P., Alkhamis, N., and Han, J. C., 2011, "Heat Transfer and Pressure Drop Measurements for a Square Channel With 45 deg Round-Edged Ribs at High Reynolds Numbers," ASME J. Turbomach., **133**(3), p. 031019.
[36] Webb, R. L., Eckert, E. R. G., and Goldstein, R. J., 1971, "Heat Transfer and Friction in Tubes With Repeated-Rib Roughness," Int. J. Heat Mass Transfer, **14**(4), pp. 601–617.
[37] Wildgoose, A. J., Thole, K. A., Sanders, P., and Wang, L., 2021, "Impact of Additive Manufacturing on Internal Cooling Channels With Varying Diameters and Build Directions," ASME J. Turbomach., **143**(7), p. 071003.
[38] Reinhart, 2011, *Industrial CT & Precision*, Application of CT Scanning in Industry, Heidelberg, Germany.
[39] Hay, N., Lampard, D., and Khaldi, A., 1994, "Coefficient of Discharge of 30° Inclined Film Cooling Holes With Rounded Entries or Exits," International Gas Turbine and Aeroengine Congress and Exhibition, The Hague, Netherlands.
[40] Bunker, R. S., and Bailey, J. C., 2001, "Film Cooling Discharge Coefficient Measurements in a Turbulated Passage With Internal Crossflow," ASME J. Turbomach., **123**(4), pp. 774–780.
[41] Kays, W. M., Crawford, M. E., and Weigand, B., 2004, *Convective Heat & Mass Transfer*, McGraw-Hill, Inc., Boston, MA, 260–271.
[42] Dyson, T. E., McClintic, J. W., Bogard, D. G., and Bradshaw, S. D., 2013, "Adiabatic and Overall Effectiveness for a Fully Cooled Turbine Vane," Turbo Expo: Turbine Technical Conference and Exposition, San Antonio, TX.
[43] Figliola, R., and Beasley, D., 1995, *Theory and Design for Mechanical Measurements*, John Wiley & Sons, Hoboken, NJ, 171–209.
[44] Siemens Digital Industries Software, 2021, "Simcenter STAR-CCM+," 2021.3 (16.06.008-R8).
[45] Jones, F. B., Fox, D. W., and Bogard, D. G., 2019, "Evaluating the Usefulness of RANS in Film Cooling," Turbo Expo: Turbomachinery Technical Conference and Exposition, Phoenix, AZ.
[46] Haven, B. A., Yamagata, D. K., Kurosaka, M., Yamawaki, S., and Maya, T., 1997, "Anti-Kidney Pair of Vortices in Shaped Holes and Their Influence on Film Cooling Effectiveness," International Gas Turbine and Aeroengine Congress and Exhibition, Orlando, FL.
[47] Williams, R. P., Dyson, T. E., Bogard, D. G., and Bradshaw, S. D., 2013, "Sensitivity of the Overall Effectiveness to Film Cooling and Internal Cooling on a Turbine Vane Suction Side," ASME J. Turbomach., **136**(3), p. 031006.